



Electroplating Kinetic of Nanostructured Selenium Films from Citrate Bath

Oualid Dilmi¹ · Mohamed Benaicha¹ · Rabah Asseli¹

Received: 7 July 2020 / Accepted: 5 November 2020 / Published online: 3 January 2021
© The Tunisian Chemical Society and Springer Nature Switzerland AG 2021

Abstract

In this work; Cyclic-Voltammetry (CV) and Electrochemical Impedance Spectroscopy (EIS) were used to study the electro-deposition kinetic of selenium films in potentiostatic mode from aqueous solution containing selenium dioxide and sodium citrate at pH = 4.2. Semiconducting proprieties of obtained deposits were investigated by Mott-Schottky measurements whereas the optical ones were performed by UV–Visible spectrophotometry. The morphological characterization was carried out using the scanning electron microscopy (SEM). The obtained results showed that the electrodeposition process of selenium films in citrate bath occurred under diffusional regime as rate-limiting step. Deposition rate of selenium layers on platinum substrate is much superior than in the case of ITO substrate and up to a value of $0.65 \mu\text{g}/\text{cm}^2 \text{ s}$. The $\text{HSeO}_3^-/\text{Se}$ system becomes more rapid with the increase of the bath temperature. Obtained deposits are photoactive films that belong to p-type semiconductors with number of charge carriers in order of $10^{21}/\text{cm}^3$ and energy band gap about 1.7 eV. The grains of electroplated films have spherical forms, nanometric sizes and strong adhesion on the substrate surface.

Keywords Electrodeposition · Selenium · Nanostructure · Citrate bath · Semiconductor · Deposition rate

Abbreviations

E	Potential	α	Absorption coefficient
E^0	Standard potential	d	The thickness
i	Current density	h	Planck constant
C	Concentration	ν	Frequency
D	Diffusion coefficient	t	Transmittance
v	Scan rate	R	Reflexing coefficient
a	Transfer coefficient	n_R	Refractive index.
C_d	Double layer capacitance	C_{sc}	Capacitance of the space charge region
Z_{real}	Real part of impedance	E_{fb}	Flat band potential
Z_{im}	Imaginary part of impedance	K	Boltzmann constant
R_{tc}	Charge transfer resistance	T	Temperature
R_{el}	Electrolyte resistance	N_d	Concentration of free carrier
E_g	Energy gap	S	Electrode surface
Q	Quantity of electricity	ϵ_0	The space permittivity
z	Transferred electrons number,	ϵ	The relative dielectric
		m	Masse
		F	Faraday's constant
		r	Electrodeposition rate

✉ Oualid Dilmi
O.dilmi@univ-jijel.dz; dilmi_oualid@yahoo.fr

Mohamed Benaicha
mdbenaicha@univ-setif.dz

Rabah Asseli
mohamedrabah7070@gmail.com

¹ Energetic and Solid State Electrochemistry Laboratory, Ferhat Abbas-Setif 1 University, 19000 Sétif, Algeria

1 Introduction

Selenium (Se) is a metalloid widely present in nature, generally in association with sulfur minerals in the form of selenide or in rocks of volcanic origin. It is extracted from the

byproducts of the processing and refining of certain ores, cements, oils and many processing industries (electronics, production of glass and ceramics, rubber, plastics, pigments, lubricants, cosmetics). It is widely used in animal and human nutrition and pharmacology and it is a very important element in our life [1–3]. In addition a recent study has associated the spread of the COVID 19 to a selenium deficiency in the human body due to its deficiency in certain regions in China [4]. In recent years, electrodeposition of selenium attracted considerable attention due to its good semiconducting, optical, thermal, electric and piezoelectric properties, its use to make semiconductor compounds such as InSe, In₂Se₃ and CuInSe₂ (CIS), which have many optoelectric applications, including advanced solar cells [5–9]. Selenium appears in different phases. The amorphous phase (red, brown and black) exhibits low electronic conductivity. The crystalline phases, include several solid allotropes, namely, the rhombohedral one, the α , β and γ monoclinic ones and the trigonal (hexagonal) one. Hexagonal Se is gray and it is the densest and the most stable of all phases [10]. Nowadays, various methods are used to synthesis selenium films and its alloys [11–25]. Electrodeposition method of thin films is considered among the promising ways, due to its ability to control the thickness, it allows obtaining a large-area deposition. It is a simple process, characterized by good adhesion, reproducibility and a low cost fabrication process [26]. Several studies have used the electrodeposition methods to make electrodeposited selenium and its alloys [23, 27–37]. These methods need a careful study to search the ideal conditions for making pure selenium layer with very good optoelectronic properties in order to meet the desired industrial needs. The biggest problem that we face frequently during the electrodeposition process, is the adherence problem; which depends on several factors, among them, the grain size. The deposits with large germs are not suitable in electroplating because the lack of cohesion between them and the little covering of the substrate surface whereas the deposit with small germs have a good adherence owing to the good cohesion between the germs. For this reason, herein we investigate thoroughly the electrodeposition process of selenium films and its kinetics aspect during the germ growth. We also examine the ideal conditions and kinetic factors (bath composition, temperature, pressure, concentration, deposition rate and pH value) that help to obtain deposits with small granules to meet the requirements of the nanomanufacturing and nanotechnology industry on the one hand and to strengthen the cohesion of the deposited films on the other hand. The electrodeposition kinetic of red selenium on platinum substrate from citrate bath containing selenium dioxide SeO₂ was studied using electrochemical (voltammetry, electrochemical impedance spectroscopy) and physicochemical (UV–Visible spectrophotometry, scanning electron microscopy) methods. The deposition rate, the flat

band potential E_{fb} , the free carrier concentration N_d , the energy gap E_g and the grain size were also investigated.

2 Experimental

Red selenium dioxide SeO₂ (Sigma–Aldrich) and sodium citrates tribasic dihydrate C₆H₅Na₃O₇•2H₂O (Fluka) powders are used to prepare the electrodeposition bath. Electrochemical measurements (voltammetry, electrochemical impedance spectroscopy) were carried out using Voltalab PGZ 301 controlled by computer (software VoltaMaster 4) with a cell of three electrodes; the saturated calomel electrode (SCE) as reference electrode, the platinum wire as counter electrode, the work electrode was used as platinum ($S = 0.5 \text{ cm}^2$) which was cleaned in the nitric acid during a few minutes and rinsed with distilled water before each manipulation. In the case of electrodeposition on ITO (indium tin oxide) substrate we have used a square plate ($S = 1 \text{ cm}^2$) cleaned in acetone for 5 min, then in the nitric acid (30%) during 2 min and finally well rinsed with distilled water.

In this study, we used for all handling an aqueous solution of 50 mM selenium dioxide SeO₂ which dissolves in water and gives HSeO₃[−] according to pourbaix diagram [38] with 0.15 M sodium citrates at ambient temperature, The pH = 4.2 was controlled by digital high precision pH-meter (HANNA instruments brand) and adjusted as needed by adding some drops of concentrated hydrochloric acid solution (HCl). The surface morphology of electrodeposited films was investigated by a JSM-6360 SEM. The UV–VIS transmittance spectrums have been recorded with a Shimadzu UV-1800 UV–Visible Scanning Spectrophotometer. The semiconducting properties of selenium deposited films on platinum were studied using the Mott-Schottky measurements in (0.1 M) KCl aqueous solution with 0.5 kHz employed frequency.

In the case of Mott-Schottky measurements the deposited films were elaborated on platinum substrates to ensure that the analyzed junction is Se/electrolyte and not ITO/electrolyte, but in the optical and micrographic analysis, the films were electrodeposited on the ITO substrates.

3 Results and Discussion

In order to verify the electrochemical behavior of the electrodeposition bath; firstly we have used the cyclic voltammetry to check the electrochemical processes which may occur in the electrolytic solution of the electrodeposition. Figure 1 shows a cyclic voltammogram of an aqueous solution containing SeO₂ (50 mM) and sodium citrate medium (0.15 M) plotted on platinum electrode at pH = 4.2 with scanning rate of 5 mV s^{−1}.

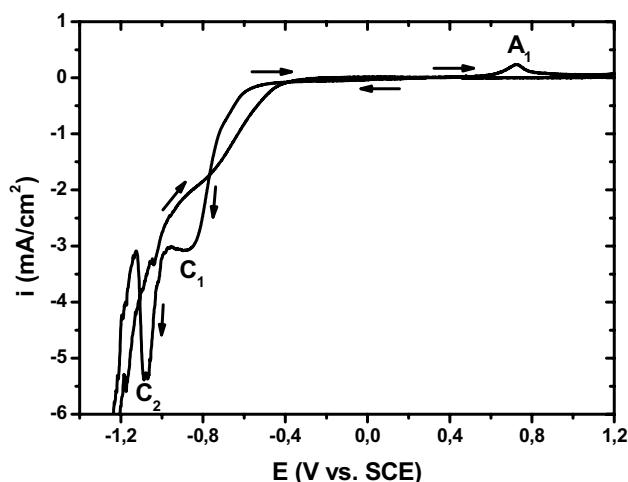
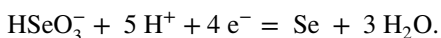
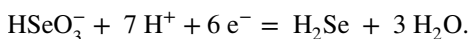


Fig. 1 Voltammogram of SeO_2 aqueous solution (50 mM) in medium of sodium citrate (0.15 M) ($T=20\text{ }^\circ\text{C}$, $\text{pH}=4.2$) plotted on platinum electrode with scanning rate $v=5\text{ mV s}^{-1}$

In this figure, scanning the potential from more positive values towards the cathodic side, we can observe two cathodic peaks C_1 (at -0.885 V vs. SCE) and C_2 (at -1.076 V vs. SCE) which are related respectively to the formation of (Se) electrodeposited and release of H_2Se gas [according to Eqs. (1) and (2)] (chemical formation of elemental selenium can also take place). In the return scan we can see an anodic peak A_1 (at 0.72 V vs. SCE) corresponds to the oxidation of electrodeposited selenium. It is obvious that the reduction peak is greater than the oxidation one; this confirms that the deposited quantity was not oxidized completely, but a small part of it only. In addition; the great spacing between the reduction and oxidation peaks which translated by the irreversibility of $\text{HSeO}_3^-/\text{Se}$ system [26–28, 39–41]. In the reverse scan, it is clear that the current density is higher than during the forward scan between -0.7 and -0.4 V which shows that the electrodeposited selenium film on the platinum substrate follows the three dimensional nucleation and growth mode. The intersection point during a reverse scan is the beginning of the germination process. In the case of cathodic polarization on ITO substrate in acid medium; the irreversible electroreduction of the tin oxide can also take place [42].



$$E^0 = 0.778 - 0.0739\text{ pH} + 0.0148\text{ log} [\text{HSeO}_3^-] \quad (1)$$



$$E^0 = 0.386 - 0.0690\text{ pH} + 0.0098\text{ log} \left(\frac{[\text{HSeO}_3^-]}{[\text{H}_2\text{Se}]} \right) \quad (2)$$

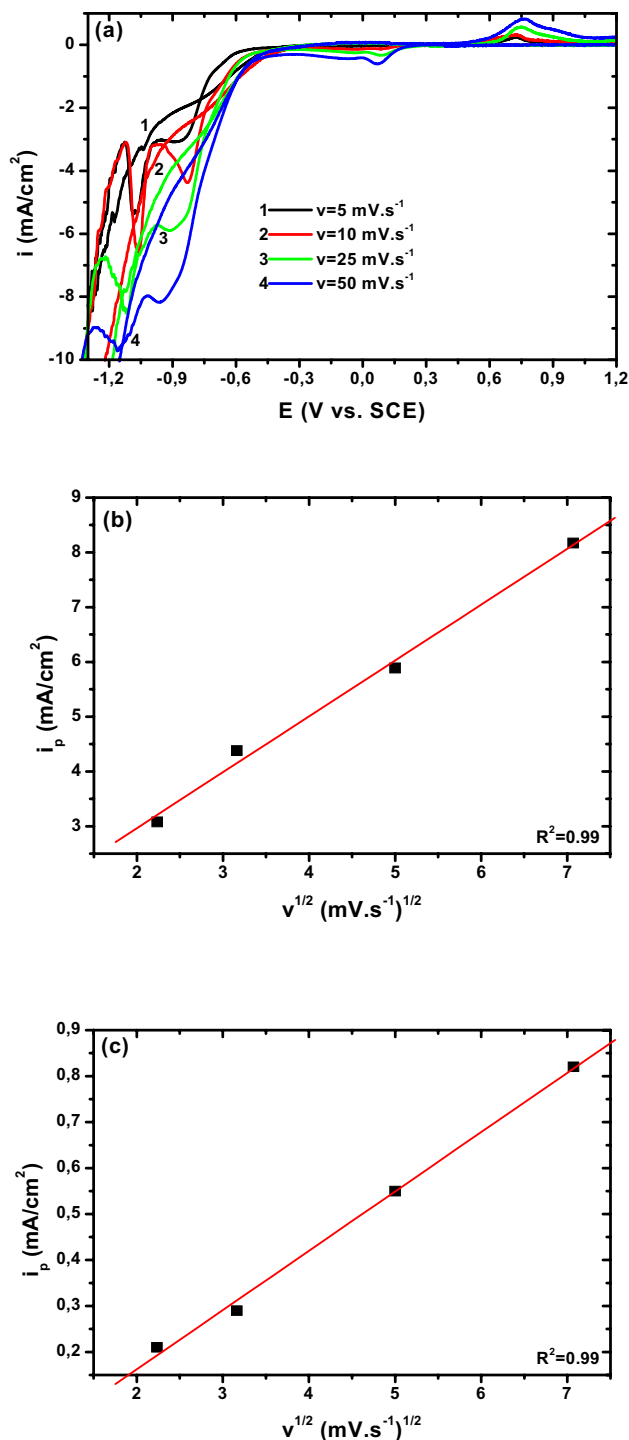


Fig. 2 Cyclic voltammograms of SeO_2 aqueous solution (50 mM) with sodium citrate (0.15 M) ($T=20\text{ }^\circ\text{C}$, $\text{pH}=4.2$), traced on platinum electrode at various scan rates (a), with the plots i vs. $v^{1/2}$ for b cathodic and c anodic peaks

Figure 2 presents the effect of scan rate on the electrochemical behavior of electroplating bath on platinum electrode accompanied by the variation of the critical current density according to the square root of the scan rate. We

can observe that the increase of the potential scan rate v increases the current density of peaks corresponding to formation and dissolution of selenium C_1 and A_1 and shifts potentials of peaks to the cathodic C_1 and the anodic A_1 sides. When we reach great rates the reduction peak of the dissolved oxygen in the electrolytic medium can be seen in the cyclic voltammogram at 0.07 V vs. SCE. Fig. 2b, c confirmed the linear variation of the current density of cathodic and anodic peaks with the square root of the scanning rate according to Eq. (3), which well showed that the diffusion of the electroactive species is the limitation step of the deposition and oxidation processes of selenium films [43].

$$i_{crit} = 2.99 \cdot 10^5 z \sqrt{az} \cdot C \sqrt{D} \sqrt{v} = B \cdot \sqrt{v} \quad (3)$$

Such as: a the transfer coefficient, z the number of electrons transferred, C concentration, D the diffusion coefficient.

The effect of bath temperature on the electrochemical behavior was also studied. The Fig. 3 shows cyclic voltammograms set of SeO_2 aqueous solution (50 mM) with sodium citrate (0.15 M) traced on platinum electrode with scan rate of 5 V m s^{-1} at $\text{pH} = 4.2$ and different temperatures (20, 40, 60 and 80 °C). In this figure it is clear that the increase of the bath temperature gives different shapes of the voltammograms but the same peaks were observed in all cases. Variation of the shape and increase of peaks in voltammograms with increasing of the bath temperature can be explained by an increase in the activity and movement of electroactive species in the electrolytic solution and the increase in the thermal agitation. We can also see that the increase of bath temperature shifts the potentials of peaks towards small values (oxidation and reduction peaks become

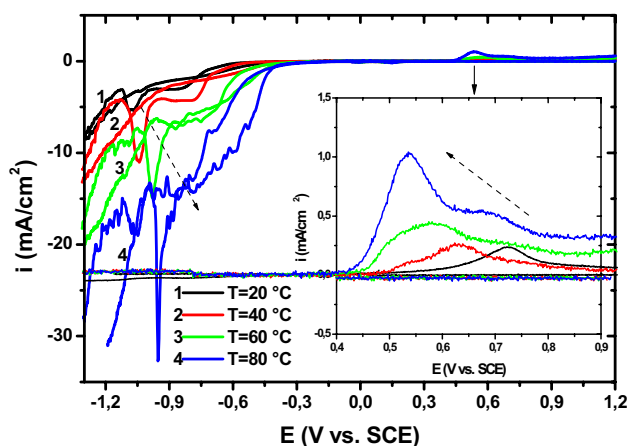


Fig. 3 Cyclic voltammograms of selenium dioxide aqueous solution (50 mM) with sodium citrate (0.15 M) traced on platinum electrode with scan rate 5 mV S^{-1} at $\text{pH} = 4.2$ and different temperatures

closer to each other); i.e. the reverse of the scanning rate influence. In this case we can say that the increase of the bath temperature makes the system more rapid (rapidity of $\text{HSeO}_3^-/\text{Se}$ system increases owing to the increase in diffusion rate of electroactive species under the effect of the increase in temperature bath which considered the limiting step rate of the selenium electrodeposition process i.e. the limiting stage of the system speed).

Figure 4 shows the Nyquist impedance measurements for different deposition potentials of selenium on platinum electrode in the frequency range 50 kHz to 100 MHz. We can see the decrease of faradic loops (semi-circle) with the increase in deposition applied potential due to the increase in deposition rate; indicating that the formed layers of selenium have a small charge transfer resistance compared with the platinum surface knowing that the deposited amount increases with increasing applied potential to more negative values (i.e. the coverage of platinum surface by the electrodeposited selenium increases). We can also observe in this figure small inductive loops at low frequencies for certain applied potentials due to the adsorption of the electrolytic solution species on the electrode surface (probably the citrate ion). The electrochemical impedance response of the electrodeposition process of selenium can be modeled by an equivalent electric circuit containing capacitor, two resistances and coil [44–46]. Table 1 outlines the average values of electrolyte resistance R_{el} , charge transfer resistance R_{tc} and double-layer capacitance C_d for each value of deposition potential.

Table 2 shows the recorded quantity of electricity values Q during the electrodeposition process of selenium films in potentiostatic mode at different applied potentials ($\text{pH} = 4.2$, $T = 20 \text{ °C}$) on platinum and ITO substrates for 10 min. In order to ensure that the quantity of electricity recorded by

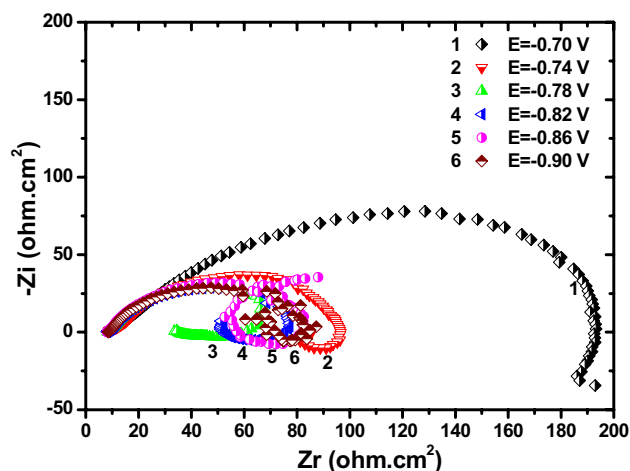


Fig. 4 Nyquist diagrams of selenium electrodeposition on platinum electrode from SeO_2 aqueous solution (50 mM) in medium of sodium citrates (0.15 M) ($\text{pH} = 4.2$, $T = 20 \text{ °C}$)

Table 1 Values of electrolyte resistance R_{el} , charge transfer resistance R_{tc} and double-layer capacitance C_d for each deposition potential of selenium films

E (V vs. SEC)	C_d ($\mu\text{F}/\text{cm}^2$)	R_{el} (ohm. cm^2)	R_{tc} (ohm. cm^2)
– 0.70	40.25	10.94	121.3
– 0.74	51.98	10.67	98.06
– 0.78	57.28	9.31	76.45
– 0.82	65.94	8.57	80.71
– 0.86	71.64	8.46	77.84
– 0.90	64.25	8.61	75.81

the potentiostat is consumed only by the electrodeposition of selenium films, the working electrode was monitored during the electrodeposition process in order to ensure that no gas bubbles are emitted (the Nyquist diagrams in electrochemical impedance spectroscopy analysis can prove this, when the electrodeposition is accompanied by a noisy release of hydrogen or other gas the shape of the diagram is greatly distorted). Here it should be noted that the value of the quantity of electricity registered by the potentiostat at – 0.9 V vs. SCE applied potential was all consumed in the selenium electrodeposition, but after this potential value $E < -0.9$ V, we begin to notice the release of gas bubbles on the work electrode, which means that in this case the process of electrodeposition was accompanied by the release of gases that may be hydrogen or H_2Se i.e. there is an interference between the electrodeposition of selenium and other parasitic reactions, for this reason the set of electrodeposition samples was stopped at this potential value (– 0.9 V) and we took the quantity of electricity as an approximation as it was all consumed in the selenium electrodeposition. As we can observe in the table; the consumed amount of electricity increases with the increase of applied potential. The deposition rate r and the thickness d of deposited film relating to each sample were calculated using Faraday’s law (Eq. 4), it is obvious that the electrodeposition rate of selenium on platinum substrate is very great compared to its electrodeposition rate on the ITO, this is mainly due to the significant difference in conductivity between platinum and tin oxide on the one hand. On the other hand, the lack

of active sites on the surface of ITO substrate, with the possibility that not all of the surface was activated during the activation process with nitric acid solution.

$$m = \frac{QM}{zF} \tag{4}$$

Figure 5 presents the Mott-Schottky measurements of selenium thin films electrodeposited in potentiostatic mode on the platinum substrate at different applied potentials for 10 min. the basis of this method is the formation of Schottky barrier between the semiconductor material and electrolytic solution [47–49]; it involves measuring the capacitance of the space charge region (C_{sc}) according to electrode tension according the flow equation [50]:

$$\frac{1}{C_{sc}^2} = \frac{2}{\epsilon\epsilon_0 N_d S^2} \left(E - E_{fb} - \frac{kT}{e_0} \right) \tag{5}$$

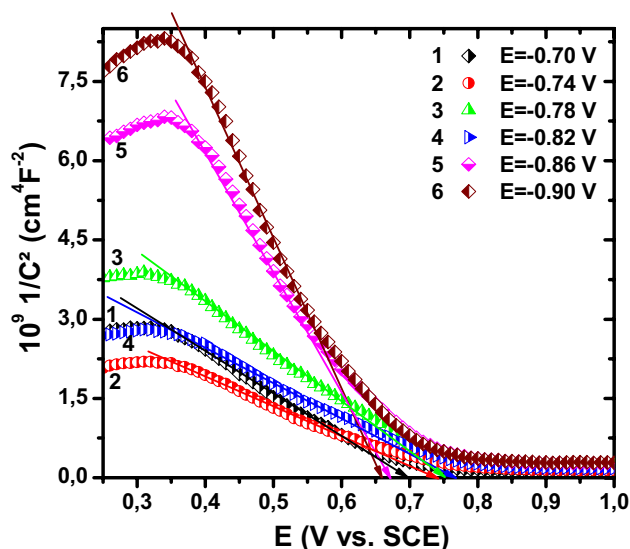


Fig. 5 Mott–Schottky plots for electrodeposited selenium at different potentials from SeO_2 aqueous solution (50 mM) in medium of sodium citrates (0.15 M) (pH=4.2, T=20 °C). In all cases the employed frequency was 0.5 kHz

Table 2 Values of quantity of electricity Q , deposition rate r and thickness d corresponding to each applied potential during electrodeposition of selenium on platinum and ITO substrates

E (V vs. SEC)	Se/Pt			Se/ITO		
	Q (mC/cm ²)	r ($\mu\text{g}/\text{cm}^2$ s)	d (μm)	Q (mC/cm ²)	r ($\mu\text{g}/\text{cm}^2$ s)	d (μm)
– 0.70	478	0.16	0.23	34.78	0.011	0.016
– 0.74	1173	0.39	0.55	42.15	0.014	0.020
– 0.78	1635	0.55	0.77	45.11	0.015	0.021
– 0.82	1331	0.45	0.63	53.57	0.018	0.025
– 0.86	1745	0.59	0.83	75.79	0.025	0.036
– 0.90	1921	0.65	0.91	86.75	0.030	0.041

where ϵ_0 is the space permittivity (8.85×10^{-14} F cm⁻¹), ϵ is the relative dielectric of elemental selenium (6.7), N_d is the concentration of the free carrier in the semiconductor, S is the area in contact with the electrolyte, E is the applied potential, E_{fb} is the flat band potential, K is the Boltzmann constant (1.38×10^{-23} J k⁻¹), T is the absolute temperature (293 K), and e_0 is the charge of electron. The plot of $1/C_{SC}^2$ as a function of applied potential E for a plane semiconductor can be permitted to determine the nature of the semiconductor material n or p as well as the determination of the its electronic properties (the density of the donor and acceptor charge carriers, and the flat band potential).

In this figure, we can observe that all samples exhibited negative slopes, indicating the P-type characteristic of the obtained (Se) semiconductor. The slope of the tangent line in Mott-Schottky plots is proportional to the $1/N_d$; and the intersection of this tangent line with the abscissa axis gives us the flat band potential. Table 3 outlines the experimental values of flat band potential E_{fb} and the concentration of free carrier N_d relating to each sample.

Determination of the transition type direct or indirect, as well as the investigation of the energy gap value of a semiconductor can be carried out by UV–Visible spectrophotometry. The semiconductor materials absorb the light at certain wavelength λ_g which can be related to the gap according the follow relationship [51]:

$$\lambda_g(nm) = \frac{1240}{E_g} (eV) \quad (6)$$

The extinction of corresponding light follows an exponential law

$$I = I_0 \exp(-\alpha l) \quad (7)$$

where l is the penetration length of the light and α is the optical absorption coefficient, this last is a function with the thickness d , the transmittance t and the reflexing coefficient of the semiconductor material R ; it can be expressed by the following formula [52–55].

$$\alpha = \frac{1}{d} \ln \left[\frac{(1-R)^2}{2t} + \left(\frac{(1-R)^4}{4t^2} + R^2 \right)^{1/2} \right] \quad (8)$$

The reflexing coefficient can be given by the following equation:

$$R = \frac{(n_R - 1)^2}{(n_R + 1)^2} \quad (9)$$

n_R is the refractive index.

On the other hand the absorption coefficient is a function to the energy of incident photons ($h\nu$) and the energy gap E_g , according the following formula [56]:

$$\alpha h\nu = A(h\nu - E_g)^n \quad (10)$$

A is a constant depends to the refractive index, the reduced mass and the light speed in the vacuum. The exponent n depends to the transition type:

For a direct gap (direct transition) $n = 0.5$

For an indirect gap (indirect transition) $n = 2$.

So, in order to investigate the semiconducting properties of each semiconductor materials, it's possible to plot the curve:

$$(\alpha h\nu)^{1/n} = f(h\nu) \quad (11)$$

The intersection of the affine part of this curve and the horizontal axis give us the value of energy gap E_g .

The transmittance spectrums UV–Visible of selenium films electrodeposited in potentiostatic mode on ITO substrate at different applied potentials, and the plot $(\alpha h\nu)^2$ vs. $(h\nu)$ are presented on the Fig. 6. This figure shows that the deposited films of selenium are photoactive materials in the UV–Visible range which translates by the observed transmission bands. The plot $(\alpha h\nu)^2$ vs. $(h\nu)$ is valid to estimate the energy gap value according to Eq. (11) ($n = 0.5$ for the red and gray selenium thin layers [57]), from this equation when $\alpha h\nu$ tends towards zero $h\nu$ tends towards E_g , which leads that extrapolation on the axis $(h\nu)$ gives us directly the energy gap value of the analyzed material. The thicknesses of obtained selenium films at these potentials were used to get the absorption coefficient values α from the transmittance values t . Energy gap values E_g according to applied deposition potential are outlined in Table 4; These energy gap values are comparable to those reported in the literature (1.93–2.0 eV by AL-ANI et al. [58], 1.83–1.96 eV by Bhatnagar et al. [59], 1.76 eV by Chaudhuri et al. [60] and 1.86 eV by Fochs [61]).

Morphological characterization of the electrodeposited film was carried out in order to get an idea about microstructure of deposited selenium as well as the grain forms and the

Table 3 The flat band potential and the free carrier density (cm⁻³) values of electrodeposited selenium on platinum substrate at different applied potentials

E (V vs. SCE)	- 0.70	- 0.74	- 0.78	- 0.82	- 0.86	- 0.90
E_{fb} (V vs. SCE)	0.69	0.74	0.75	0.77	0.67	0.66
$10^{-21} \times N_d$ (cm ⁻³)	1.63	2.33	1.94	1.34	0.62	0.49

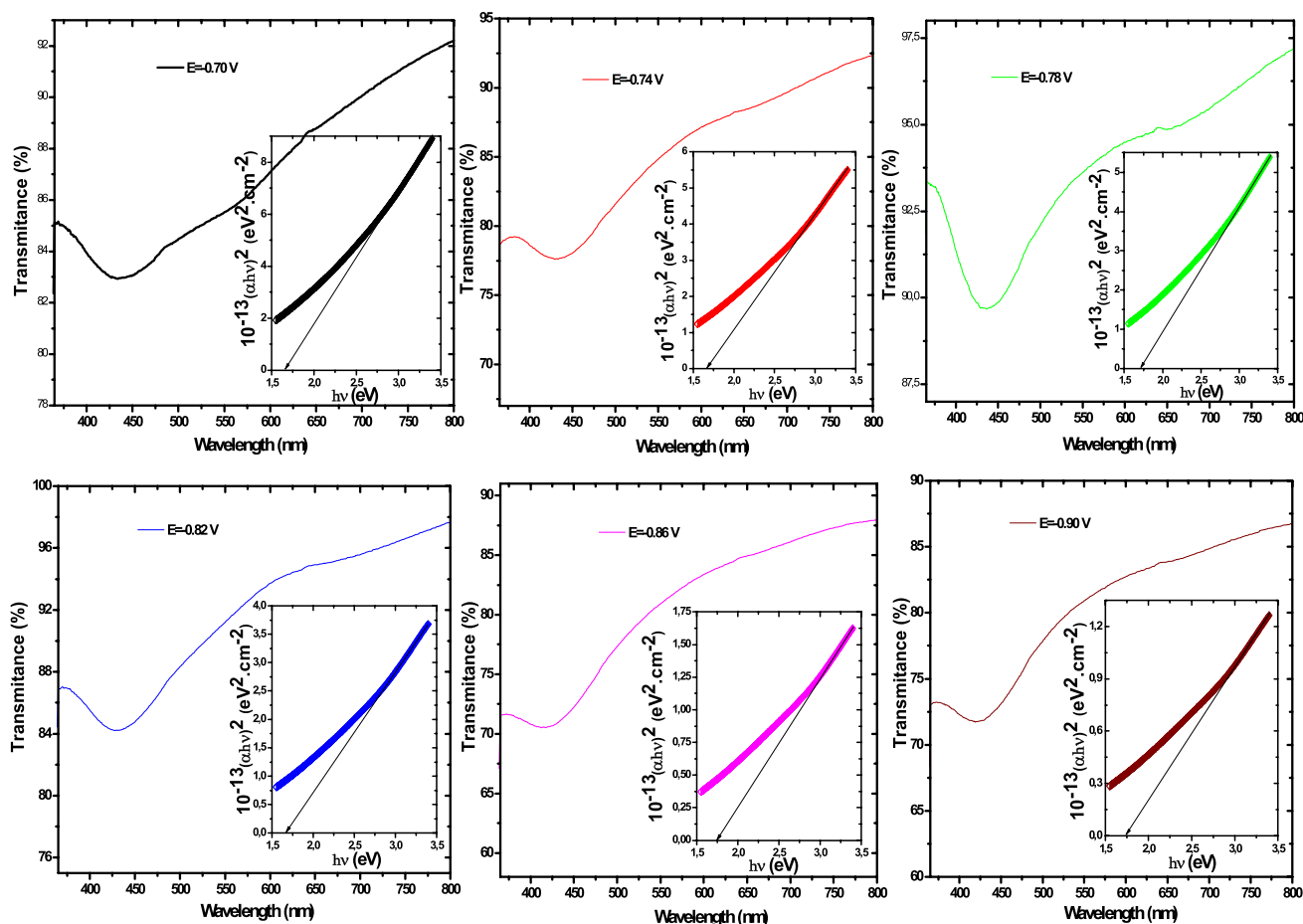


Fig. 6 UV–Visible transmittance spectrums of electrodeposited selenium films on the ITO substrate during 10 min at different applied potentials (pH=4.2, T=20 °C) with the plot $(\alpha h\nu)^2$ vs. $(h\nu)$

Table 4 Values of energy gap E_g according to applied potentials

E (V vs. SEC)	– 0.70	– 0.74	– 0.78	– 0.82	– 0.86	– 0.90
E_g (eV)	1.64	1.66	1.70	1.66	1.75	1.74

grain size. Figure 7 shows scanning electron microscopy (SEM) image of electrodeposited selenium sample obtained at – 0.86 V vs. SCE applied potential on ITO substrate during 10 min in potentiostatic mode. It is clear that this obtained deposit is less dense and composed from spherical grains forms with nanometric grain in different sizes. We can also see the formation of germs with dimensions ranging from 2 to 2.5 μm contain about 15–25 grains. In this case it can be ensure that the cohesion between the grains is greatest and their coverage of the surface is strong even if we increase the time of the electrodeposition process, which can give a deposited film with good adherence. To confirm this good adherence, a simple mechanical test using sandpaper was carried out accompanied with chemical test by dipping the sample in a solution of nitric acid; it was finding that for

complete stripping of the deposited film, a strong concentration was required.

4 Conclusion

The electrodeposition kinetic of selenium on platinum and ITO substrates from citrate bath was studied in this paper; from the obtained results it can be recorded that: Electrodeposition of selenium occurs under the diffusional control regime as limitation step. Deposition rate of selenium films on platinum substrate is superior than in the case of ITO substrate and up to a value of 0.65 $\mu\text{g}/\text{cm}^2\cdot\text{s}$. The increase of the bath temperature makes the system $\text{HSeO}_3^-/\text{Se}$ more rapid. Electrodeposited layers are

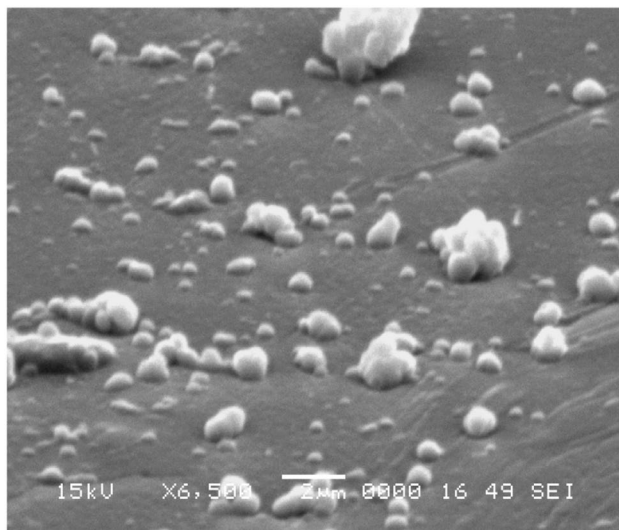


Fig. 7 SEM Image of electrodeposited selenium film on ITO substrate at applied potential -0.86 V vs. SCE during 10 min (pH=4.2, $T=20$ °C)

photoactive films and belongs to p-type semiconductors with number of charge carriers in order of $10^{21}/\text{cm}^3$ and energy gap about 1.7 eV. The grains of electroplated films have spherical forms and nanometric sizes with strong adhesion on the surface substrate.

The recorded results would help us understand the kinetic and the good conditions for electrodeposition of selenium films with nano-grains and good adherence on the substrate surface and open up prospects for research on the same axis.

Acknowledgements This work was supported by the Energetic and Solid State Electrochemistry Laboratory (Ferhat Abbas-Setif1 University-Algeria); the authors would like to thank ZAIM Keltoum and DERBAL Sabrina for their assistances.

Compliance with Ethical Standards

Conflict of interest The authors declare that they have no conflict of interest.

References

1. Khurana A, Tekula S, Saifi MA, Venkatesh P, Godugu C (2019) *Biomed Pharmacother* 111:802. <https://doi.org/10.1016/j.biopha.2018.12.146>
2. Kuria A, Fang X, Li M, Han H, He J, Aaseth JO, Cao Y (2020) *Crit Rev Food Sci Nutr* 60:684. <https://doi.org/10.1080/10408398.2018.1548427>
3. Huo B, He J, Shen X (2020). *Biol Trace Elem Res*. <https://doi.org/10.1007/s12011-020-02070-6>
4. Zhang J, Taylor EW, Bennett K, Saad R, Rayman MP (2020) *Am J Clin Nutr* 111:1297. <https://doi.org/10.1093/ajcn/nqaa095>

5. Gates B, Mayers B, Cattle B, Xia Y (2002) *Adv Funct Mater* 12:219. [https://doi.org/10.1002/1616-3028\(200203\)12:3%3c219::AID-ADFM219%3e3.0.CO;2-U](https://doi.org/10.1002/1616-3028(200203)12:3%3c219::AID-ADFM219%3e3.0.CO;2-U)
6. Tan SH, Kounaves SP (1998) *Electroanalysis* 10:364. [https://doi.org/10.1002/\(SICI\)1521-4109\(199805\)10:6%3c364::AID-ELAN364%3e3.0.CO;2-F](https://doi.org/10.1002/(SICI)1521-4109(199805)10:6%3c364::AID-ELAN364%3e3.0.CO;2-F)
7. Ferri T, Sangiorgio P (1999) *Anal Acta* 385:337. [https://doi.org/10.1016/S0003-2670\(98\)00693-X](https://doi.org/10.1016/S0003-2670(98)00693-X)
8. Badr Y, Mahmoud MA (2005) *Phys B* 369:278. <https://doi.org/10.1016/j.physb.2005.08.027>
9. Kowalik R, Fitzner K (2009) *J Electroanal Chem* 633:78. <https://doi.org/10.1016/j.jelechem.2009.04.029>
10. Kargar Razi M, Maamoury RS, Banihashemi S (2011) *Int J Nano Dim* 1:261. <https://doi.org/10.7508/IJND.2010.04.003>
11. Gurin VS, Prokopenko VB, Alexeenko AA, Wang Sh, Prokoshin PV (2001) *Mater Sci Eng C* 15:93. [https://doi.org/10.1016/S0928-4931\(01\)00267-3](https://doi.org/10.1016/S0928-4931(01)00267-3)
12. Jiang H, Yao X, Che J, Wang M, Kong F (2004) *Ceram Int* 30:1685. <https://doi.org/10.1016/j.ceramint.2004.03.030>
13. Zhang W, Chai Y, Cao N, Wang Y (2014) *Mater Lett* 134:123. <https://doi.org/10.1016/j.matlet.2014.07.072>
14. Chen Y, Zhang W, Fan Y, Xu X, Zhang Z (2006) *Mater Chem Phys* 98:191. <https://doi.org/10.1016/j.matchemphys.2005.05.051>
15. Wang Z, Chen X, Liu J, Yang X, Qian Y (2003) *Inorg Chem Commun* 6:1329. <https://doi.org/10.1016/j.inoche.2003.08.009>
16. Martínez-Escobar D, Ramachandran M, Sánchez-Juárez A, Narro Rios JS (2013) *Thin Solid Films* 535:390. <https://doi.org/10.1016/j.tsf.2012.12.081>
17. Ubale AU, Sakhare YS (2014) *Vacuum* 99:124. <https://doi.org/10.1016/j.vacuum.2013.05.004>
18. Jiang X, Mayers B, Wang Y, Cattle B, Xia Y (2004) *Chem Phys Lett* 385:472. <https://doi.org/10.1016/j.cplett.2004.01.033>
19. Zhang S-Y, Zhang J, Liu Y, Ma X, Chen H-Y (2005) *Electrochim Acta* 50:4365. <https://doi.org/10.1016/j.electacta.2005.01.044>
20. Pola J, Bastl Z, Subrt J, Ouchi A (2001) *Appl Surf Sci* 172:220. [https://doi.org/10.1016/S0169-4332\(00\)00851-5](https://doi.org/10.1016/S0169-4332(00)00851-5)
21. Mendoza D, Lpez S, Granados S, Morales F, Escudero R (1997) *Synth Met* 89:71. [https://doi.org/10.1016/S0379-6779\(97\)81195-2](https://doi.org/10.1016/S0379-6779(97)81195-2)
22. Abdel Aal A, Voigts F, Chakarov D, Endres F (2012) *Electrochim Acta* 59:228. <https://doi.org/10.1016/j.electacta.2011.10.064>
23. Maranowski B, Strawski M, Osowiecki W, Szklarczyk M (2015) *J Electroanal Chem* 752:54. <https://doi.org/10.1016/j.jelechem.2015.05.037>
24. Cabral MF, Suffredini HB, Pedrosa VA, Tanimoto ST, Machado SAS (2008) *Appl Surf Sci* 254:5612. <https://doi.org/10.1016/j.apsusc.2008.03.038>
25. Steichen M, Dale P (2011) *Electrochem Commun* 13:865. <https://doi.org/10.1016/j.elecom.2011.05.023>
26. Lai Y, Liu F, Li J, Zhang Z, Liu Y (2010) *J Electroanal Chem* 639:187. <https://doi.org/10.1016/j.jelechem.2009.11.026>
27. Cattarin S, Furlanetto F, Musiani MM (1996) *J Electroanal Chem* 415:123. [https://doi.org/10.1016/S0022-0728\(96\)04707-9](https://doi.org/10.1016/S0022-0728(96)04707-9)
28. Zein El Abedin S, Saad AY, Farag HK, Borisenko N, Liu QX, Endres F (2007) *Electrochim Acta* 52:2746. <https://doi.org/10.1016/j.electacta.2006.08.064>
29. Ivanov DK, Poznyak CK, Osipovich NP, Strel'tsov EA (2004) *Russ J Electrochem* 40:1044. <https://doi.org/10.1023/B:RUEL.0000046489.81407.ff>
30. Kowalik R, Kazimierzczak H, Żabiński P (2016) *Mater Sci Semicond Process* 50:43. <https://doi.org/10.1016/j.mssp.2016.04.009>
31. Kwiecińska AM, Kutyla D, Kołczyk-Siedlecka K, Skibińska K, Żabiński P, Kowalik R (2019) *J Electroanal Chem* 848:113278. <https://doi.org/10.1016/j.jelechem.2019.113278>
32. Coelho D, Luiz GM, Machado SAS (2018) *J Electroanal Chem* 820:89. <https://doi.org/10.1016/j.jelechem.2018.04.050>

33. Rasche B, Amin HMA, Clarke SJ, Compton RG (2019) *J Electroanal Chem* 835:239. <https://doi.org/10.1016/j.jelechem.2019.01.015>
34. Xu J, Wang W, Zhang X, Chang X, Shi Z, Haarberg GM (2015) *J Alloys Compd* 632:778. <https://doi.org/10.1016/j.jallcom.2015.01.013>
35. Whyte GM, Awada C, Offor PO, Otung FU, Alshoabi A, Aljaafari A, Ekwealor ABC, Maaza M, Ezema FI (2020) *Opt Mater* 99:109556. <https://doi.org/10.1016/j.optmat.2019.109556>
36. Majidzade VA, Aliyev AS, Guliyev PH, Babanly DM (2020) *J Electrochem Sci Eng* 10:1. <https://doi.org/10.5599/jese.676>
37. Ye X, Chen L, Liu L, Bai Y (2017) *Mater Lett* 196:381. <https://doi.org/10.1016/j.matlet.2017.03.072>
38. Pourbaix M (1963) *Atlas d'équilibre électrochimique à 25°C*, p:557
39. Santos MC, Machado SAS (2004) *J Electroanal Chem* 567:203. <https://doi.org/10.1016/j.jelechem.2003.12.026>
40. Cavallini M, Aloisi G, Guidelli R (1999) *Langmuir* 15:2993. <https://doi.org/10.1021/la981231a>
41. Pourbaix M (1963) *Atlas d'équilibre électrochimique à 25°C*, pp:555–556
42. Senthilkumar M, Mathiyarasu J, Joseph J, Phani KLN, Yeg-naraman V (2008) *Mater Chem Phys* 108:403. <https://doi.org/10.1016/j.matchemphys.2007.10.030>
43. Bard AJ, Faulkner LR (2001) *Electrochemical methods: fundamentals and applications*. Wiley, New York
44. Wiart R (1990) *Electrochim Acta* 35(10):1587. [https://doi.org/10.1016/0013-4686\(90\)80014-F](https://doi.org/10.1016/0013-4686(90)80014-F)
45. Gassa LM, Mishima HT, de Mishima BAL, Vilche JR (1997) *Electrochim Acta* 42(11):1717. [https://doi.org/10.1016/S0013-4686\(96\)00371-4](https://doi.org/10.1016/S0013-4686(96)00371-4)
46. Fan Y, Yang J, Jiang L, Wang Y, Ng BK, Sun H, Lai Y, Li J, Liu F (2017) *J Electrochem Soc* 164(4):H225. <https://doi.org/10.1149/2.1481704jes>
47. Rousset J, Saucedo E, Lincot D (2009) *Chem Mater* 21:534. <https://doi.org/10.1021/cm802765c>
48. Windisch CF, Exarhos GJ (2000) *J Vac Sci Technol* 18:1677. <https://doi.org/10.1116/1.582406>
49. Mora-Seró I, Fabregat-Santiago F, Denier B, Bisquert J, Tena-Zaera R, Elias J, Lévy-Clément C (2006) *Appl Phys Lett* 89:203117. <https://doi.org/10.1063/1.2390667>
50. Morrison SR (1980) *Electrochemistry at semiconductor and oxidized metal electrodes*. Plenum Press, New York
51. Hagfeldt A, Graetzel M (1995) *Chem Rev* 95:49. <https://doi.org/10.1021/cr00033a003>
52. González-Hernández J, Gorley PM, Horley PP, Vartsabyuk OM, Vorobiev YV (2002) *Thin Solid Films* 403–404:471. [https://doi.org/10.1016/S0040-6090\(01\)01543-7](https://doi.org/10.1016/S0040-6090(01)01543-7)
53. Yamaguchi T, Yamamoto Y, Tanaka T, Tanahashi N, Yoshida A (1998) *Sol Energy Mater Sol Cells* 50:1. [https://doi.org/10.1016/S0927-0248\(97\)00091-3](https://doi.org/10.1016/S0927-0248(97)00091-3)
54. Huang CJ, Meen TH, Lai MY, Chen WR (2004) *Sol Energy Mater Sol Cells* 82:553. <https://doi.org/10.1016/j.solmat.2003.12.008>
55. Sadigov MS, Özkan M, Bacaksiz E, Altunbaş M, Kopya AI (1999) *J Mater Sci* 34:4579. <https://doi.org/10.1023/A:1004670112975>
56. Singh RP, Singh SL, Chandra S (1986) *J Phys D: Appl Phys* 19:1299. <https://doi.org/10.1088/0022-3727/19/7/019>
57. Pejova B, Grozdanov I (2001) *Appl Surf Sci* 177:152. [https://doi.org/10.1016/S0169-4332\(01\)00191-X](https://doi.org/10.1016/S0169-4332(01)00191-X)
58. Al-ani SKJ, Al-delaimi MN, Abdul Munaim AH, Jawher HM (1990) *Int J Electron* 69:87. <https://doi.org/10.1080/00207219008920294>
59. Bhatnagar AK, Reddy KV, Srivastava V (1985) *J Phys D: Appl Phys* 18:L149. <https://doi.org/10.1088/0022-3727/18/9/001>
60. Chaudhuri S, Biswas SK, Choudhury A, Goswami K (1983) *J Non-Cryst Solids* 54:179. [https://doi.org/10.1016/0022-3093\(70\)90026-8](https://doi.org/10.1016/0022-3093(70)90026-8)
61. Fochs PD (1956) *Proc Phys Soc London Sect B* 69:70. <https://doi.org/10.1088/0370-1301/69/1/309>